

Unified Stress-Strain Model for Plasticity to the Structural Instability

Alan F. Jankowski¹

¹ Sandia National Laboratory, Livermore, CA USA

Correspondence: Alan F Jankowski, Sandia National Laboratory, Materials Division, PO Box 969, Livermore, California, 94551-0969 USA. Tel: 1-925-294-2742. E-mail: afjanko@sandia.gov

Received: February 6, 2025

Accepted: February 20, 2025

Online Published: March 4, 2025

doi:10.5539/jmsr.v14n1p1

URL: <https://doi.org/10.5539/jmsr.v14n1p1>

Abstract

A unified model for the work hardening $\Theta(\sigma)$ and stress-strain $\sigma(\epsilon)$ behavior is presented that accounts for deformation under tensile loading, from the onset of yielding at the proportional limit up to the ultimate strength as defined at the structural instability. The origin of this approach is based on a negative exponential formulation for an asymptotic-curvilinear work-hardening model that accounts for the rapid strengthening of metals as well as the continuation of steady-state deformation to the instability.

Keywords: work hardening model, stress-strain model, softening coefficient

1. Introduction

The early stage of work hardening, i.e. the rapid rise in stress concurrent with small changes in strain beyond the elastic limit, has often been associated with a Hollomon (1945) formulation that's based on a power law expression for $\sigma(\epsilon)$. The limitation of this approach is seen where an asymptotic leveling of stress with increasing deformation is not possible using the power law formulation for $\sigma(\epsilon)$. Neither is an accompanying asymptotic leveling in the work hardening value $\Theta(\sigma)$ with increasing stress. The later stage of work hardening is characterized by a leveling of both $\sigma(\epsilon)$ and $\Theta(\sigma)$ to asymptotic values. This stage is often associated with a Voce (1948) formulation that's based on a negative exponential expression for $\sigma(\epsilon)$. The work hardening behavior that corresponds to the Voce expression is associated with a first-order derivative formulation (Jankowski 2023) that produces the linear Kocks and Mecking (2003) $\Theta(\sigma)$ expression. However, the limitation of this approach is that the linear Kocks-Mecking (KM) expression approximates a curvilinear work hardening $\Theta(\sigma)$ behavior. In addition, the early stage of work hardening, as typified by a rapid increase in $\sigma(\epsilon)$ and a simultaneous rapid decrease in $\Theta(\sigma)$, can't be modeled solely using the Voce-based $\sigma(\epsilon)$ formulation.

A closed-form analytic model is now proposed that recognizes the curvilinear $\Theta(\sigma)$ behavior and provides a mechanism to represent the rapid rise in stress which is followed by an asymptotic leveling. A negative exponential formulation provides an Arrhenius-type behavior in $\Theta(\sigma)$. This approach uses Boltzmann statistics to account for changes encountered during loading with increasing disorder to the microstructure during deformation, as often typified by dislocation mobilization, generation and annihilation. A simultaneous rapid rise in strength beyond the proportional limit to a gradual steady-state range of plasticity is well modeled (Jankowski, et al. 2019, Jankowski 2021, Jankowski 2024) as seen in the recent example for the tensile behavior of the additively manufactured (AM) Ti-6Al-4V alloy. However, a limitation is the use of a single term for the negative exponential formulation of $\Theta(\sigma)$, and the concurrent natural logarithmic formulation for $\sigma(\epsilon)$, wherein the transition occurs rapidly from the early to later stages of work hardening. For instance, the Ti-6Al-4V alloy is a case where the tensile behavior is characterized by limited ductility to the instability point. Herein, the $\Theta(\sigma)$ behavior is significantly affected by initial (Stage 3) work hardening behavior and consequently the use of a single $\Theta(\sigma)$ formulation is found (Jankowski 2024) to be sufficient for an integral formulation of $\sigma(\epsilon)$.

Therefore, a single stage-based formulation of $\Theta(\sigma)$ is likely to be deficient for materials with an extended range of plasticity, where an overestimation of strength occurs beyond the yield point and prior to the instability. To remedy this circumstance, the base $\Theta(\sigma)$ formulation (Jankowski 2023) is now proposed as being effective to model both early and later stages of work hardening through use of multiple $\Theta(\sigma)$ terms, i.e. one for Stage 3 as well as one for Stage 4. Analogous to the addition of bulk and grain-boundary diffusion terms, the Arrhenius formulation of $\Theta(\sigma)$ is effective for all Stage behaviors. As the Stage 3 $\Theta(\sigma)$ values rapidly descend, the Stage 4 $\Theta(\sigma)$ terms for steady-state work hardening continue the plastic deformation to the strength instability. Such is

the case as seen in experimental findings for stainless steel alloys as 304L (Jankowski and Yee 2023) and 316L (Jankowski, et al. 2020). The single formulation can underestimate the ultimate strength when modeled to fit the proportional limit or, conversely, overestimate the rise in strength that occurs after the proportional limit is reached when modeled to fit the ultimate strength. To address this limitation, a unified model is now considered to envelope both Stage 3 and 4 work hardening behaviors.

The unified model superposes multiple terms of the closed-form formulation (Jankowski 2023) for the analytically derived negative exponential equation for $\Theta(\sigma)$. That is, one term applies for the early stage of plasticity, and second term applies to the later stage. The summation of these terms provides a continuous variation with stress, as opposed to segmented stages. In brief, the onset of dislocation generation dominates the first term as fitted in application to the rapid rise in strength $\sigma(\varepsilon)$ and the rapid decrease in $\Theta(\sigma)$, whereas the annihilation of dislocations dominates the second term, as fitted to the asymptotic leveling of $\sigma(\varepsilon)$ and $\Theta(\sigma)$ in an apparent near steady-state range of extended plasticity. By analogy, the Arrhenius formulation for diffusion in solids can be considered (Jankowski, et al. 2005) a superposition of bulk diffusion that dominates at high temperature with grain boundary diffusion that dominates at lower temperatures. To test the postulate of superposition, a case study is presented to assess the work hardening behavior of 316L AM stainless steel.

2. Background and Analysis Method

2.1 Work hardening and stress-strain relationships

The relationship for the plastic strain ε_p between the proportional limit σ_p and strength at the instability σ_u has been derived by J.W. Morris, Jr. (2007) as formulated in eqn. (1).

$$\varepsilon_p = c_b^{-1} \cdot \ln[1 + c_b \cdot (1 - \sigma^*)] \quad (1)$$

In this expression, the integral solution for Stages 3 and 4 of work hardening is considered, wherein Stage 3 is typically associated with the rapid rise in work hardening as seen in the Hollomon power-law stress-strain expression and Stage 4 is associated with the leveling in work hardening as seen in the Voce negative-exponential stress-strain expression. The Voce expression corresponds with the work hardening relationship associated with the Kocks and Mecking (2003) formulation for $\Theta(\sigma)$ of $\Theta_o - c_b \cdot \sigma$. The softening coefficient c_b of eqn. (1) is formulated (Morris, Jr. 2007) as a function of the plastic strain ε_p from the onset of deformation at σ_p to the strength instability σ_u . This eqn. (1) formulation provides an integrated linear equivalence for the slope of the work hardening relation $\Theta(\sigma)$ as determined from the measurements of ε_p and σ^* that equals (σ_p/σ_u) .

Beyond the linear approximation for $\Theta(\sigma)$, the base formulation for a negative-exponential relationship of work hardening with true stress is seen in eqn. (2) wherein the energetic driving force is the applied stress. This Arrhenius-type formulation offers the advantage of providing a building block to track both the early to later stages of work hardening that can't be determined from other closed-form solutions of analytic models for stress-strain behavior, such as Hollomon and Voce.

$$\Theta_j(\sigma) = c_{1j} \cdot e^{-(c_{2j}\sigma)} \quad (2)$$

A rapid descent in $\Theta(\sigma)$ is associated with larger values for c_{1j} (and c_{2j}) as opposed to a smaller magnitude in $\Theta(\sigma)$ and shallower descent. The first-order differential of the work hardening curve as shown in eqn. (3) equates c_{bi} with the (negative of) slope at any point on the $\Theta(\sigma)$ curve, and manifests the change in the softening coefficient c_{bi} as will be encountered from the outset of Stage 3 (where i equals 3) to the end of Stage 4 (where i equals 4).

$$c_{bi} = -[\partial\Theta_j(\sigma)/\partial\sigma] = c_{1j} \cdot c_{2j} \cdot e^{-(c_{2j}\sigma_i)} \quad (3)$$

Following the eqn. (3) formulation for c_{bi} , a negative exponential relationship can be anticipated between the softening coefficients computed at the beginning of Stage 3 and end of Stage 4. The ratio $c_{b4}:c_{b3}$ would tend to increase as the difference $(\sigma_u - \sigma_p)$ between the stress limits decreases in magnitude. That is, c_{b4} would increase and c_{b3} decrease when the difference between the yield and ultimate strengths decreases (as is coincident with an increase in the proportional limit).

An integral of the negative-exponential work hardening expression from eqn. (2) provides a description inclusive of both Stages 3 and 4, in the following formulation of eqn. (4) as derived (Jankowski 2023) for the stress-strain relationship.

$$\sigma_j(\varepsilon) = (1/c_{2j}) \cdot \ln[c_{2j} \cdot (c_{1j} \cdot \varepsilon + c_{oj})] + \sigma_o \quad (4)$$

That is, a single expression can be used as the basis to model the entire stress-strain response and as will be explored, the Stage 3 and 4 portions can be treated separately producing c_{1j} , c_{2j} and c_{oj} values that are unique

to each Stage. An increase in c_{2j} will progressively flatten the stress-strain $\sigma_j(\varepsilon)$ curve, and an increase in c_{1j} will compound this effect. In these constitutive equations (2) and (4), the integral derivation allows the variable σ to be replaced by $(\sigma + \sigma_o)$ where σ_o is a constant, and c_{oj} is determined by eqn. (5).

$$c_{oj}(\theta_j, \varepsilon) = c_{1j} \cdot \{[1/(c_{2j} \cdot \theta_j)] - \varepsilon_i\} \quad (5)$$

By computing c_{oi} at the proportional limit σ_p for a specific true stress-strain curve, the simulation of the stress-strain curve using eqn. (4) will then include the proportional limit as appropriate for Stage 3. The total plasticity between the initial σ_i and final σ_f stress values of a work hardening range can be solved from eqn. (5) for comparison to the measured value of $(\varepsilon_{ult} - \varepsilon_{pro})$.

$$\varepsilon_p = [e^{(c_{2j} \cdot \sigma_f)} - e^{(c_{2j} \cdot \sigma_i)}] / (c_{1j} \cdot c_{2j}) \quad (6)$$

If a single constitutive stress-strain relationship is used to describe the entire range of plasticity to the instability, then proportional limit σ_p equals σ_i and the strength at the instability σ_u equals σ_f . For the treatment of individual work hardening Stages 3 and 4 to comprise the plastic deformation to the instability, the contributions from each stage components to eqns. (2) and (4) are summed and the following (J) equations result.

$$\theta_j(\sigma) = \sum [c_{ij} \cdot e^{-(c_{2j} \cdot \sigma)}] \quad (7)$$

$$\sigma_j(\varepsilon) = \sum \{ (1/c_{2j}) \cdot \ln [c_{2j} \cdot (c_{1j} \cdot \varepsilon + c_{oj})] \} + \sigma_o \quad (8)$$

This following description provides a procedure to routinely model the full stress-strain curve from the cumulative parts of the work hardening curve. The onset of plastic deformation that demarks the rapid rise in stress $\sigma(\varepsilon)$, and rapid decrease in the softening factor c_{b3} as the Stage 3 slope of $\theta(\sigma)$, is fit with the negative exponential formulation of eqn. (2). The slope of a linear fit for Stage 3 using the linear Kocks-Mecking $\theta(\sigma)$ formulation, as derived from the Voce $\sigma(\varepsilon)$ expression for stress-strain behavior, will equal that c_{b3} value computed from the negative exponential formulation of $\theta(\sigma)$ at the yield point, i.e. the proportional limit. The same scenario applies for the determination of c_{b4} for Stage 4 using the linear Kocks-Mecking and negative-exponential $\theta(\sigma)$ formulations where the c_{b4} value is computed at the ultimate strength, i.e. when the strength instability σ_u equals $\theta(\sigma_u)$. The coefficients c_{ij} that are computed from the negative-exponential $\theta(\sigma)$ formulations for Stages 3 and 4 are used to establish the true stress-strain formulations $\sigma_j(\varepsilon)$ of eqn. (4), i.e. $\sigma_{s3}(\varepsilon)$ and $\sigma_{s4}(\varepsilon)$, wherein the c_{oj} values for each stage are determined at the proportional limit and strength instability, correspondingly. The net stress-strain behavior is computed by adding the $\sigma_{s3}(\varepsilon)$ and $\sigma_{s4}(\varepsilon)$ as formulated using eqn. (8).

In addition, isolated mechanisms of work hardening that can affect the post-yielding mechanical behavior, such as twinning and/or transformation induced plasticity, can be accommodated with the derivation of a constitutive formulation using a Gaussian function which is representative of that mode. The derivation and application for this solution is presented in Appendix A.

2.2 Utility of softening coefficients c_{bi}

The softening coefficients c_{bi} can provide functional constitutive relationships with material properties. The relationship between microstructural scale is seen in the derivation of the Hall-Petch relationship between grain size and the yield strength at the proportional limit σ_p as detailed in Appendix B. This relationship can be extended to the use of the softening coefficients c_{bi} as a measure of microstructural scale.

A formulation for assessing the dislocation activation volume v^* at the onset of plastic deformation is derived (Jankowski 2023) by combining the Gibbs (1969) and Cahn-Nabarro (2001) equation for activation volume with the classic Dorn relationship ($\sigma \propto \dot{\varepsilon}^m$) for the sensitivity of materials, wherein strength σ is proportional with strain-rate $\dot{\varepsilon}$ raised to a power law exponent m . The expressions derived are shown in eqns. (9-10) where the activation volume v^* is a function of the strain-rate sensitivity exponent m and softening coefficient c_{b3} at the yield point, noting T is the temperature absolute (K), k_B is Boltzmann's constant of $1.38065 \cdot 10^{-23} \text{ J} \cdot \text{K}^{-1}$, E is the elastic modulus, and θ_{o3} is the Stage 3 work hardening intercept.

$$v^* = c_{v^*} \cdot (c_{b3}/m) \quad (9)$$

$$c_{v^*} = [k_B \cdot T / (\theta_{o3} - E)] \quad (10)$$

In eqn. (9), the ratio of softening coefficient to strain-rate sensitivity $c_{b3}:m$ is proportional to the activation

volume v^* for deformation. The corresponding relationship between v^* and (c_{b3}/m) indicates that a smaller activation volume will be commensurate with materials that have a smaller c_{b3} coefficient and/or a larger strain-rate sensitivity of strength exponent m . Correspondingly, by solving the proportionality from eqn. (B.10) for c_{b3} and substituting this solution into eqn. (9), a plot of the variation of activation volume v^* with the proportional limit σ_p should produce a second-order polynomial relationship. A plot of v^* versus σ_p^{-2} should produce a linear relationship according to the proportionality in eqn. (11). Similarly, a plot of v^* versus σ should produce a decaying parabolic relationship as strength increases.

$$v^* \propto (c_{v^*}/m) \cdot (k_\sigma/\sigma_p)^2 \quad (11)$$

3. Materials, Results and Data Analysis

The multi-stage method is now applied to the new work hardening expressions of eqn. (7) to determine the eqn. (8) stress-strain behavior of 316L AM materials with an extended stage of steady-state work hardening. The tensile data for austenitic 316L stainless steel (Jankowski, et al. 2020) is now analyzed beyond the use of eqn. (1) to assess the plastic elongation as a function of the softening coefficient c_b . Samples are selected for analysis to provide yield strengths that range from less than 200 MPa to greater than 400 MPa.

3.1 Materials and Tensile Testing

The material under study was prepared (Jankowski et al., 2020) by the method of laser powder bed fusion (LPBF) using a 3-D Systems ProX300 printer where the 0.500 kW excimer laser was operated at 40% power using an in-plane hexagonal scan pattern, a $1.200 \text{ m}\cdot\text{s}^{-1}$ beam raster speed, and a succession of $40 \text{ }\mu\text{m}$ layers. The build direction is defined as the vertical z-axis whereas in-plane growth is along the x-axis roller direction. The 316L austenite source powder has a Gaussian distribution with a mean $18 \text{ }\mu\text{m}$ particle size. The tensile samples are cut from plates of 0.66, 1.17, and 1.68 mm in thickness (i.e. 0.026, 0.046 and 0.066 in, respectively), both in the rolling (x-axis) and build (z-axis) directions using electro-discharge machining. The ‘dog-bone’ shape tensile bars have a 23.4 mm (0.92 in) length and 4.6 mm (0.18 in) width, along with a gage section of 12.7 mm (0.50 in) length and 1.52 mm (0.060 in) width. Tensile testing is conducted to failure with AM surfaces in the as-deposited condition. In addition, samples were cut from wrought 316L plate machined to the same thickness values where the machined surface finish is $\sim 25 \text{ }\mu\text{m}$ (1 mil) rms. The uniaxial tensile tests are conducted using a MTS hydraulic test system operated under controlled displacement to produce a 10^{-5} s^{-1} strain rate $\dot{\epsilon}$ of 10^{-4} - 10^{-5} s^{-1} . The change in length during tensile loading is measured with a laser interferometer using reflective surface markers placed within the gage length. The results for the tensile tests are plotted in Figure 1 as true stress-strain curves.

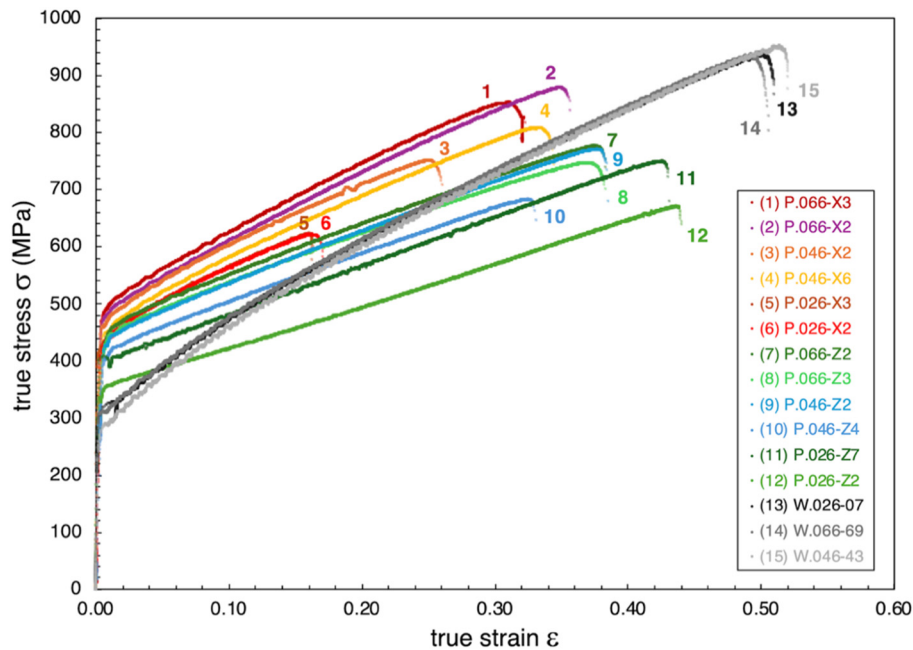


Figure 1. The true stress σ (MPa) as a function of the true strain ϵ for 316L AM and wrought material under uniaxial tensile loading

The proportional limit σ_p is used for the measure of the yield strength and is determined where the correlation coefficient R^2 for the linear elastic range in Figure 1 drops below 0.98. The ultimate strength σ_u is determined as the strength at the instability. This marks the end of the range for plastic deformation that occurs during uniform elongation for a true stress-strain plot. The value for σ_u is determined by the Considère criteria where the slope $\Theta(\sigma)$ of the $\sigma(\epsilon)$ curve equals the true stress. The σ_p , σ_u values and an 0.2% offset strength are listed in Table 1 along with the true strain ϵ_p , ϵ_u values at the proportional limit and ultimate strength.

Table 1. Tensile strength (σ_p, σ_u) and strain (ϵ_p, ϵ_u) values for AM316L

sample	eq. (1)	true stress (MPa)			true strain	
	c_b	σ_p	$\sigma_{0.2\%}$	σ_u	ϵ_{pro}	ϵ_{ult}
P.026-X2	9.25	406.7	423.7	619.8	0.0039	0.1586
P.026-X3	9.54	388.8	415.1	621.5	0.0012	0.1604
P.026-Z2	0.90	316.1	327.6	668.0	0.0020	0.4330
P.026-Z7	1.61	306.8	403.5	743.1	0.0014	0.4144
P.046-X2	6.39	291.2	421.1	750.2	0.0011	0.2501
P.046-X6	3.11	362.8	437.1	803.1	0.0033	0.3233
P.046-Z2	2.78	282.9	369.2	764.1	0.0026	0.3641
P.046-Z4	3.49	291.6	391.9	678.3	0.0039	0.3177
P.066-X2	3.38	319.7	456.6	873.4	0.0026	0.3416
P.066-X3	3.27	423.7	483.1	847.6	0.0045	0.3008
P.066-Z2	3.08	279.9	388.1	762.7	0.0031	0.3545
P.066-Z3	3.01	265.1	388.8	729.7	0.0023	0.3580
W.026-07	1.65	259.7	307.5	938.7	0.0012	0.5007
W.046-43	1.61	193.6	266.7	949.6	0.0011	0.5137
W.066-69	1.39	280.1	307.0	932.2	0.0016	0.4886

3.2 Softening Coefficients c_{bi} of Work Hardening $\Theta(\sigma)$

The softening coefficient c_b determined using the Morris, Jr. (2007) formulation of eqn. (1) for each sample is listed in Table 1 and plotted in Figure 2 versus the plastic strain ($\epsilon_{ult} - \epsilon_{pro}$) between the proportional limit and ultimate strength. Guideline values of σ^* from 0.3 to 0.6 are provided in Figure 2 as dashed lines along with $\epsilon_p(c_{b4})$ data plotted as determined using eqns. (3) and (7) to represent the end point to Stage 4 of plasticity. The amount of useful plasticity is seen to increase in Figure 2 as the c_b and c_{b4} values decrease.

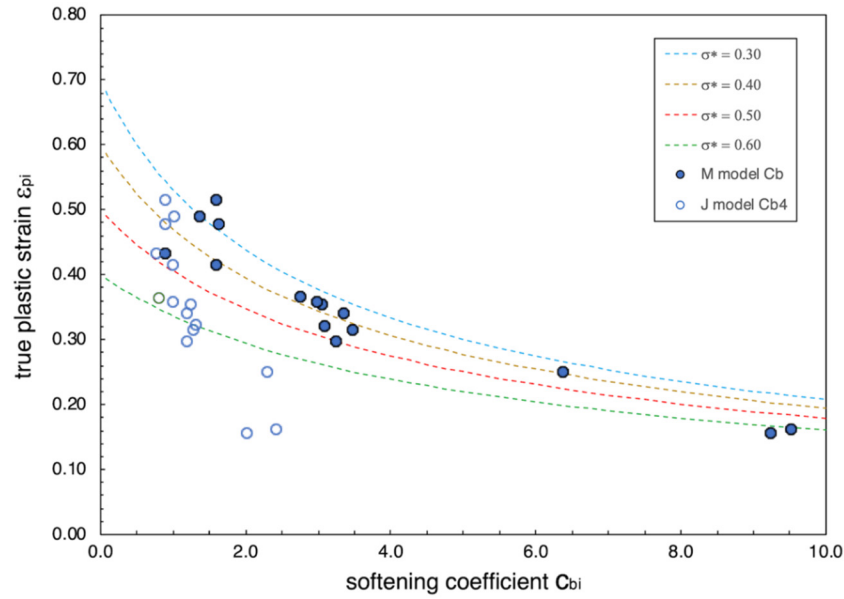


Figure 2. The plastic strain ε_p to the instability plotted as a function of the softening coefficient c_{b4} (Jankowski model c_{b4}) using the unified model of eqn. (7) and the integrated value c_b (Morris Jr. model c_b) of eqn. (1) for AM and wrought 316L samples

The use of eqn. (7) to model the work hardening from the proportional limit to the instability is shown in Figure 3 for three Figure 1 stress-strain curves as selected to represent an increasing progression in strength at the proportional limit σ_p . The c_{b3} value is determined at the beginning of Stage 3 plastic deformation at the proportional limit using the eqn. (7) fit of each Figure 3 plot, and the c_{b4} value is determined at the strength instability at the end of Stage 4. The c_{1j} and c_{2j} values are determined from the data curve fit of the work hardening using eqn. (2) for each of the Stages 3 and 4 along with the c_{oj} values as determined using eqn. (5) and the input of the c_{ij} values as computed at σ_p and σ_u . The c_{bi} and c_{ij} values are listed accordingly in Table 2 for Stages 3 and 4 as determined using the unified model of eqn. (7) input to eqn. (3), along with softening coefficients determined using the linear K-M work hardening approximation that corresponds with the Voce stress-strain model.

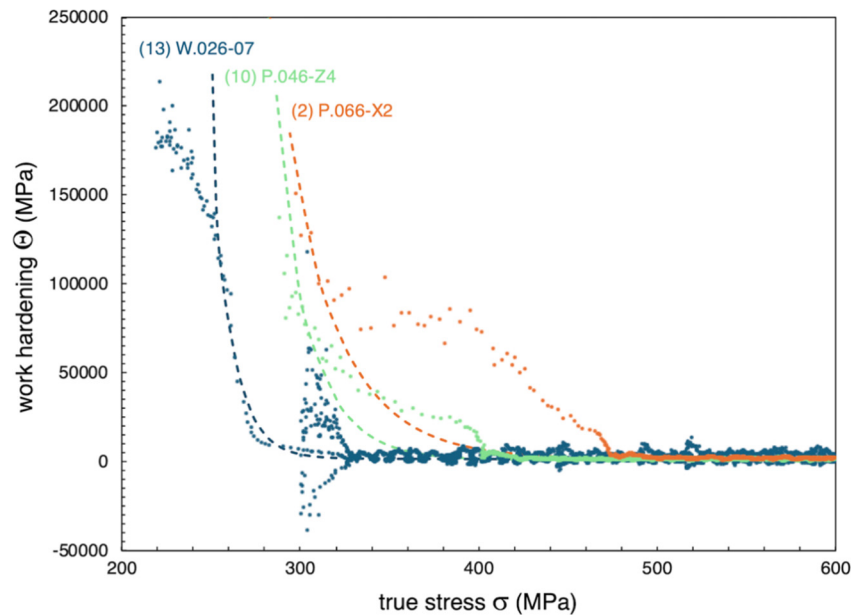


Figure 3. The work hardening Θ (MPa) variation with true stress σ (MPa) for wrought and AM 316L samples fit using the eqn. (7) negative exponential formulation of $\Theta(\sigma)$

Table 2. Softening coefficients (c_{bi} , c_{ij}) values for AM316L

sample	Stage 3						Stage 4			
	Voce		eq. (3)	MPa	MPa ⁻¹	MPa	eq. (3)	MPa	MPa ⁻¹	MPa
	c_{b3}	c_{b4}	c_{b3}	c_{1j}	c_{2j}	$-c_{oj}$	c_{b4}	c_{1j}	c_{2j}	c_{oj}
P.026-X2	2215	2.11	2477	$8.31 \cdot 10^{19}$	0.0873	$2.97 \cdot 10^{17}$	2.04	3605	0.00217	1197
P.026-X3	3369	2.58	3496	$2.41 \cdot 10^{17}$	0.0745	$2.29 \cdot 10^{14}$	2.44	4625	0.00251	1154
P.026-Z2	4130	1.11	3887	$7.10 \cdot 10^{15}$	0.0828	$1.12 \cdot 10^{13}$	0.79	1460	0.0123	1217
P.026-Z7	4268	1.05	4504	$1.56 \cdot 10^{12}$	0.0540	$1.88 \cdot 10^9$	1.01	2046	0.00150	1185
P.046-X2	3934	2.41	3962	$7.30 \cdot 10^9$	0.0384	$6.27 \cdot 10^6$	2.31	6825	0.00283	1246
P.046-X6	3455	1.39	2902	$1.48 \cdot 10^{11}$	0.0404	$4.24 \cdot 10^8$	1.34	3005	0.00158	1278
P.046-Z2	7228	0.92	7025	$3.65 \cdot 10^{16}$	0.0955	$8.86 \cdot 10^{13}$	0.81	1736	0.00103	1501
P.046-Z4	5475	1.39	6142	$2.96 \cdot 10^{11}$	0.0500	$1.11 \cdot 10^9$	1.30	2498	0.00193	1125
P.066-X2	4114	1.31	2986	$2.86 \cdot 10^9$	0.0330	$6.28 \cdot 10^6$	1.20	2935	0.00144	1440
P.066-X3	2728	1.27	2605	$3.67 \cdot 10^{12}$	0.0422	$1.52 \cdot 10^{10}$	1.21	2800	0.00123	1464
P.066-Z2	6755	1.39	7299	$6.54 \cdot 10^{18}$	0.1144	$1.94 \cdot 10^{16}$	1.26	2800	0.00185	1224
P.066-Z3	7044	1.15	6919	$2.02 \cdot 10^{16}$	0.0998	$4.35 \cdot 10^{13}$	1.02	2029	0.00150	1266
W.026-07	6187	1.04	6639	$4.08 \cdot 10^{14}$	0.0861	$4.40 \cdot 10^{11}$	0.92	2350	0.00098	1385
W.046-43	12100	0.97	11536	$1.32 \cdot 10^9$	0.0442	$1.36 \cdot 10^6$	0.91	2360	0.00095	1382
W.066-69	7016	1.08	7550	$9.04 \cdot 10^{14}$	0.0816	$1.38 \cdot 10^{12}$	1.03	2602	0.00111	1264

For a direct comparison between these methods, the c_{b3} and c_{b4} values are plotted in Figure 4 where the data points are seen to lie on the dashed line having a slope of one.

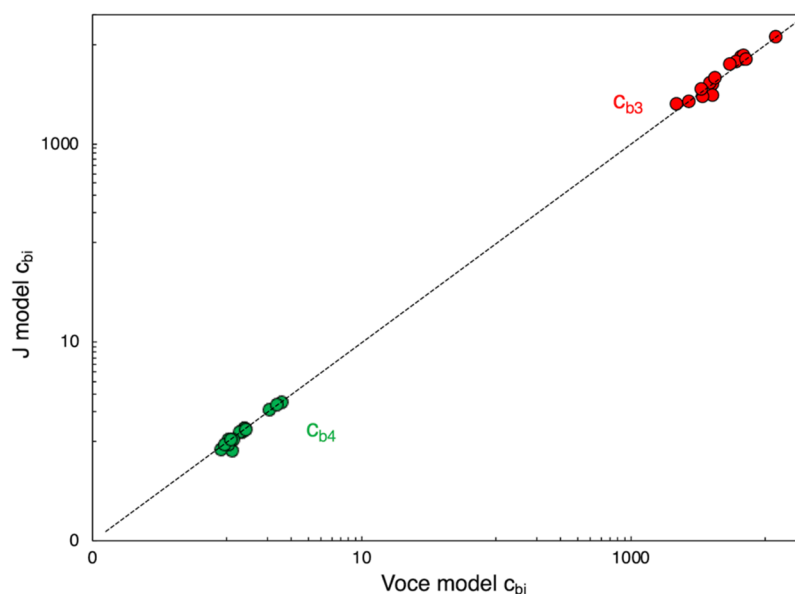


Figure 4. The c_{b3} and c_{b4} values are plotted for all AM and wrought 316L samples using eqn. (3) for the unified (J model) work hardening determination from eqn. (7), and the linear Kocks-Mecking relation for Stage 3 and 4 as based on the Voce stress-strain model

The Figure 4 results show a correspondence between point computations using the linear approximation for each stage, and the curvilinear fit of the full work hardening curve at the proportional limit and strength instability. The c_{b3} and c_{b4} values are found to differ by three-orders of magnitude for the 316L alloy. An evaluation of the

trending behavior between the c_{b3} and c_{b4} values can next be made in context to the formulation of eqn. (3), for the Table 2 data that is plotted in Figure 5.

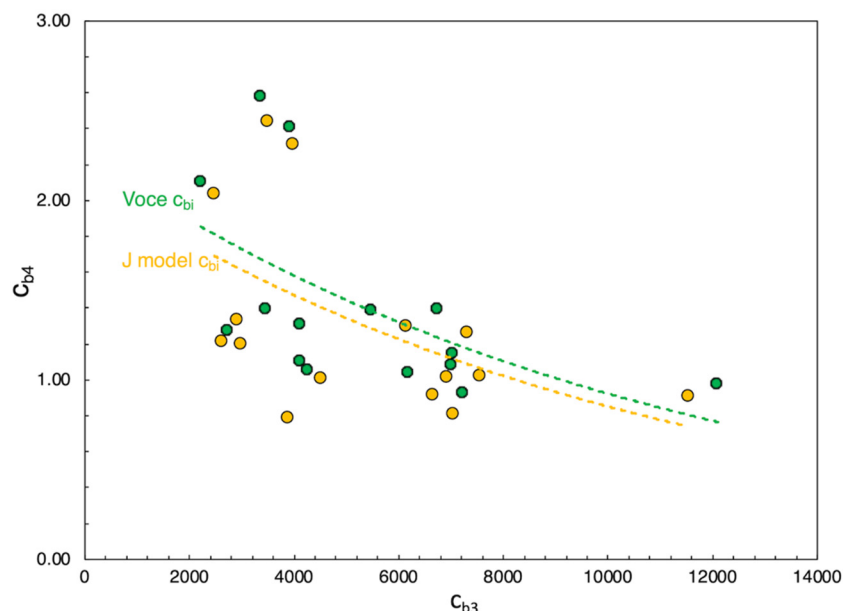


Figure 5. The variation between the softening coefficients c_{b3} and c_{b4} is plotted for values determined using the linear and negative exponential work hardening models

In general, as the proportional limit increases, the c_{b3} value is found to decrease in Figure 5 as the c_{b4} value increases in magnitude. A negative exponential relationship for the Figure 5 plot can be formulated (Jankowski 2024) or, alternatively, a more specific relationship follows from eqn. (3) where the ratio of $c_{b4}:c_{b3}$ is found to be proportional to $e^{(c_{23} \cdot \sigma_p - c_{24} \cdot \sigma_u)}$ by a factor of $(c_{14} \cdot c_{24}) / (c_{13} \cdot c_{23})$.

The fluctuations observable in the work hardening plots of Figure 3, *after* the onset of deformation in Stage 3 and *prior* to steady-state range of Stage 4, are not modeled using eqn. (7). For example, the loop in the $\Theta(\sigma)$ curve for sample no. W.026-07 represents the appearance of upper and lower yield points, as may arise attributable to solute effects on inhibiting the initiation of dislocation motion. The presence of the work hardening plateau following the $\Theta(\sigma)$ drop in Stage 3, as seen in samples no. 2 P.066-X2 and no. 10 P.046-Z4, can represent the onset of dislocation glide. The Figure 3 work hardening behavior is modeled to *envelope* these additional $\Theta(\sigma)$ fluctuations that are (often) localized immediately beyond the proportional limit and occur before the extended steady state of plasticity to Stage 4.

Additional effects, as can arise from extensive twinning and detwinning, are microstructural variants that are not directly accounted for in the statistical mechanics formulation of the work hardening model of eqns. (2-3) and (7). Beyond the basic modeling of Stages 3 and 4 using eqn. (7) that establishes the envelope to work hardening behavior and the corresponding eqn. (8) for stress-strain response, the appearance of additional work hardening stages which follow Stage 3 can be modeled using consideration of Gaussian curves component(s) for those discrete regions. Although beyond the scope of this presentation, the derivation of formulations and application examples are provided in Appendix A.

3.3 Work Hardening $\Theta(\sigma)$ -Based Stress-Strain $\sigma(\epsilon)$ Behavior

The determination of the c_{ij} coefficients from the work hardening curves for Stages 3 and 4, using eqns. (2) and (7), enables an envelope of the work hardening behavior to be established (as shown in Figure 3) that serves the basis for modeling the stress-strain behavior using eqns. (4) and (8). Details of the $\Theta(\sigma)$ contributions from the individual Stage 3 and 4 are shown in Figure 6 for sample P.066-Z2 with corresponding c_{ij} values listed in Table 1.

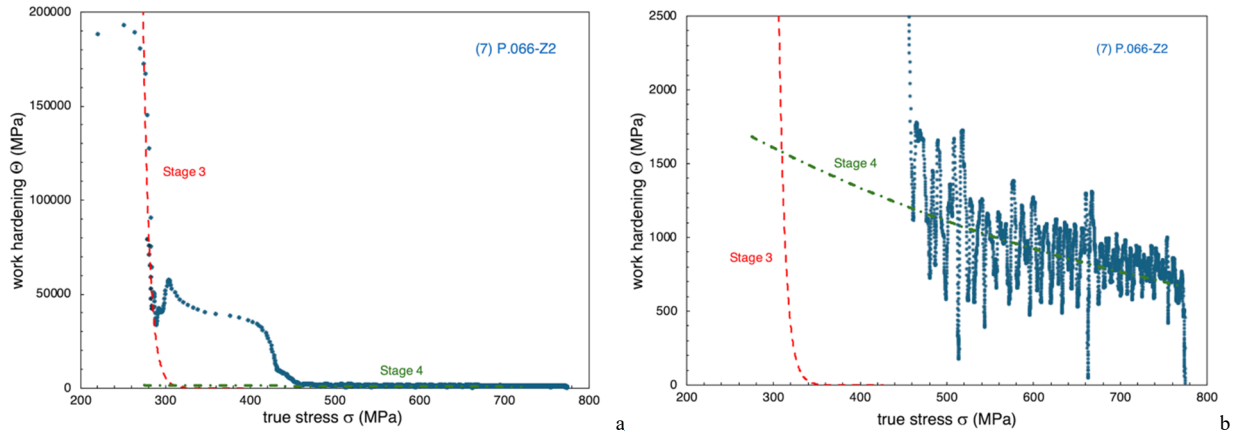


Figure 6. The application of the $\Theta(\sigma)$ formulation from eqn. (2) is used to model the individual contributions to work hardening for sample P.066-Z2 from (a) Stage 3 and (b) Stage 4

The true stress-strain $\sigma(\varepsilon)$ curves for sample P.066-Z2 are plotted in Figure 7. The experimental data (aqua curve) is shown along with curves modeled using eqn. (4) for the individual Stage 3 and 4 contributions $\sigma_{S3}(\varepsilon)$ (red curve) and $\sigma_{S4}(\varepsilon)$ (green curve), as well as the cumulative response (yellow curve) as determined by eqn. (8). The gap at low strain values between the Stage 3+4 model (yellow) and the experimental (aqua) curves in Figure 7 can be attributed to the additional work hardening behavior(s) that can follow Stage 3 and precede Stage 4 as seen in Figure 6a for sample P.066-Z2. Beyond modeling Stage 3 and 4 contributions, the effect of additional $\Theta(\sigma)$ stages to the stress-strain behavior are presented in Appendix A as determined by solving a series of partial integrals that results in a series expansion for strain as a function of applied stress $\varepsilon(\sigma)$.

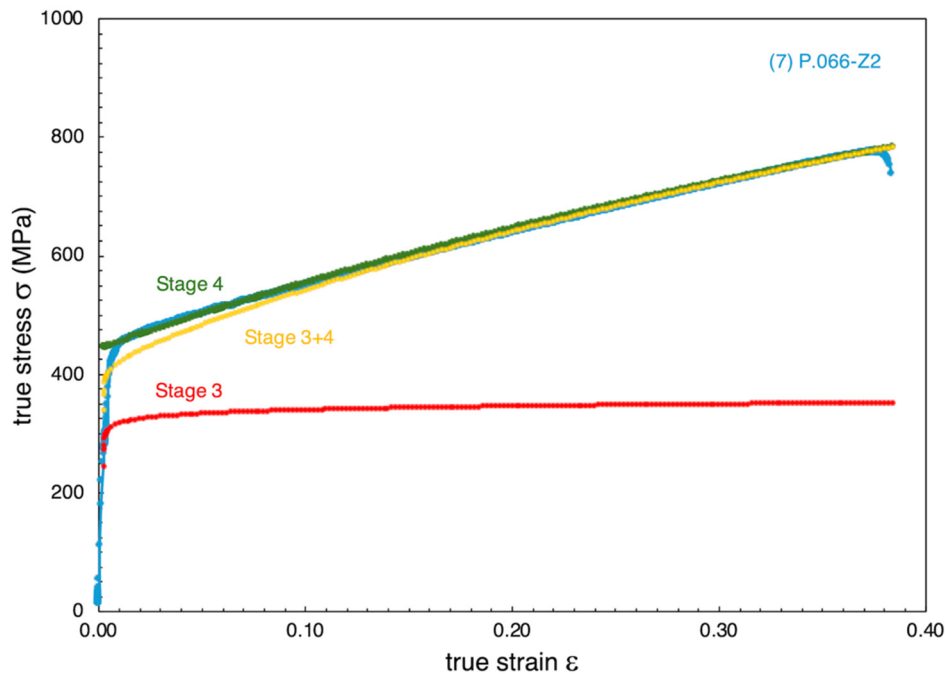


Figure 7. The true stress-strain curves for sample P.066-Z2 are plotted as experimentally measured (yellow) and as determined using eqn. (4) for work hardening contributions from individual Stages 3 (red) and 4 (green) and as determined cumulatively (yellow) using eqn. (8)

The numerical solutions for a corresponding $\sigma(\varepsilon)$ behavior that results from the Gaussian contribution to work hardening can then be applied using the c_{ij} coefficients determined for that Gaussian working hardening stage. The example shown in Appendix A is the work hardening behavior of sample P.066-X2 and the corresponding

modeling of the stress-strain response for comparison with experimental results.

3.4 Strengthening Behavior $\sigma(c_{b3})$ and Activation Volume v^*

A Hall-Petch type relationship between the softening coefficient c_{b3} and the material strength has been proposed (Jankowski 2024) as represented in eqn. (B.10) of Appendix B. A similar relationship for $\sigma(c_{b4})$ can be developed as seen in eqn. (B.13). Prior experimental evidence (Jankowski 2021, 2024) for the eqn. (B.10) Hall-Petch relationship is seen in the sequence of work hardening curves for Ti-6Al-4V where the slope c_{b3} of the $\Theta(\sigma)$ curve decreases as the proportional limit increases in value. The same progression is seen in Figure 3 work hardening curves for the 316L AM samples. The strength data for the 316L samples as a function of $\sqrt{c_{b3}}$ are now plotted in Figure 8 following the eqn. (B.10) formulation of the Hall-Petch relationship where the correlation coefficient R^2 is found to equal 0.82, the slope k_σ equals 16337 MPa, and the intercept σ_{op} equals 70 MPa.

An assessment of the activation volume v^* for the onset of deformation and strength σ can be made wherein the stress-strain curves are used to compute the variational relationship with strain rate $\dot{\epsilon}$. A linear variation of v^* as a function of c_{b3} is forecast from eqn. (9) and plotted in Figure 9 using a typical value of 0.014 for the strain-rate sensitivity exponent m of 316L. From the Figure 9 plot of eqn. (9), the correlation coefficient R^2 is found to equal 0.77 where the slope (c_{v^*}/m) equals $6.60 \cdot 10^{-5}$. Consistent to the inclusion of a Hall-Petch type relationship as seen in Figure 8 with the proportionality of $v^*(c_{b3})$ as seen in Figure 9, a plot for the formulation of eqn. (11) developed in Sec. 2.2 reveals a decaying parabolic relationship for $v^*(\sigma_p)$ in Figure 10 with a correlation coefficient R^2 of 0.96. In these plots, an average elastic modulus E of 177 ± 21 GPa is computed from the data reported in Tables 1 and 2 as measured from the true stress-strain curves. In comparison to the 193-200 GPa that is typical for 316 L, the standard deviation ΔE affects the values computed for the activation volume v^* by less than 7%.

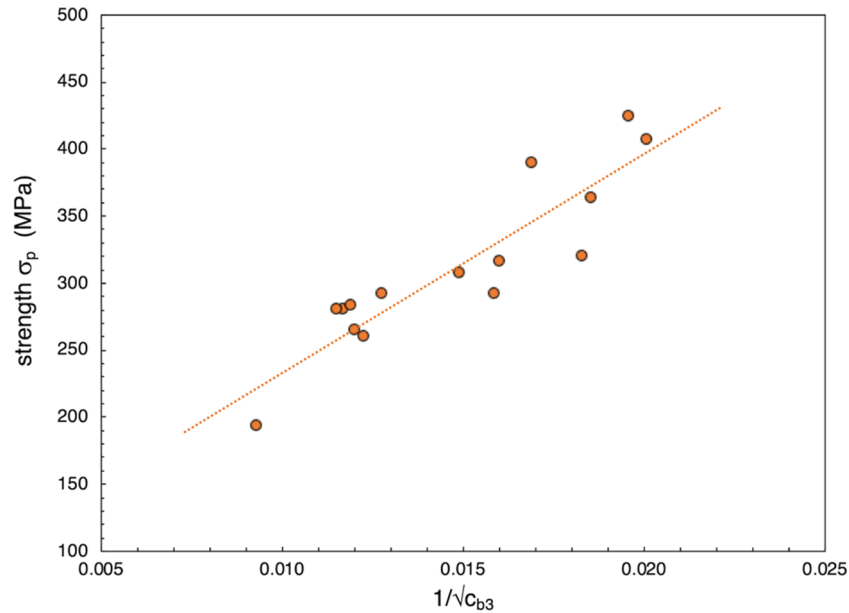


Figure 8. The tensile strength of wrought and AM 316L plotted with the proportional limit σ_p (MPa) as an inverse square-root function of the c_{b3} value that's computed from the work hardening data using the negative exponential formulation of $\Theta(\sigma)$ from eqn. (2).

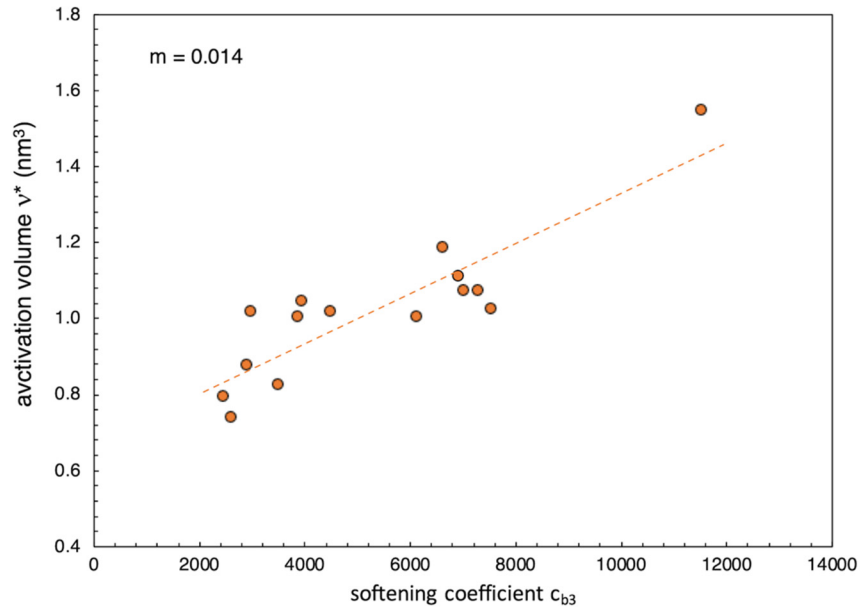


Figure 9. The activation volume ν^* for the onset of dislocation motion at the proportional limit is plotted as a function of the softening coefficient c_{b3} in accordance with eqn. (9)

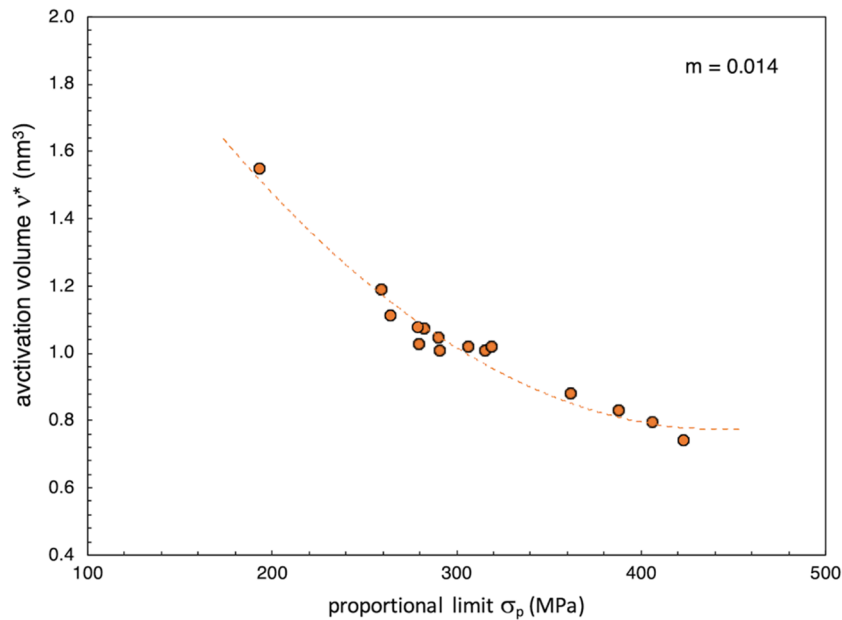


Figure 10. The activation volume ν^* is seen to be a parabolic function of the proportional limit σ_p value of strength following the formulation presented in eqn. (11)

The use of the softening coefficient c_{b3} provides a surrogate means to quantify the dimensional scale of the complex AM microstructure. During AM synthesis, the locations of first contact provide the subsequent path to solidification. Elongated grain structures within the 316L AM plate appear (Jankowski, et al. 2020) in the build direction with a more equiaxed grain structure within the build plane. As such there will be a coincident anisotropy in grain boundary size. The variation in tensile strength that's observed from the build direction to the build plane manifests this microstructural effect. For example, a scalloped-superstructure appears coincident with the solidification of melted powder for the 0.026 in-thick AM plate build structure as metallographic sectioning along the build direction (bottom to top) and as viewed in Figure 11. With the lamellar substructure as seen in Figure 11b that's often associated with post processing features typical of cold rolling (Wang, et al. 2018), this microstructure does not readily lend itself to a conventional grain size h_g quantification (Hilliard 1964, Jankowski and Wilford

1987) with a lineal intercept analysis which employs a circular test figure.

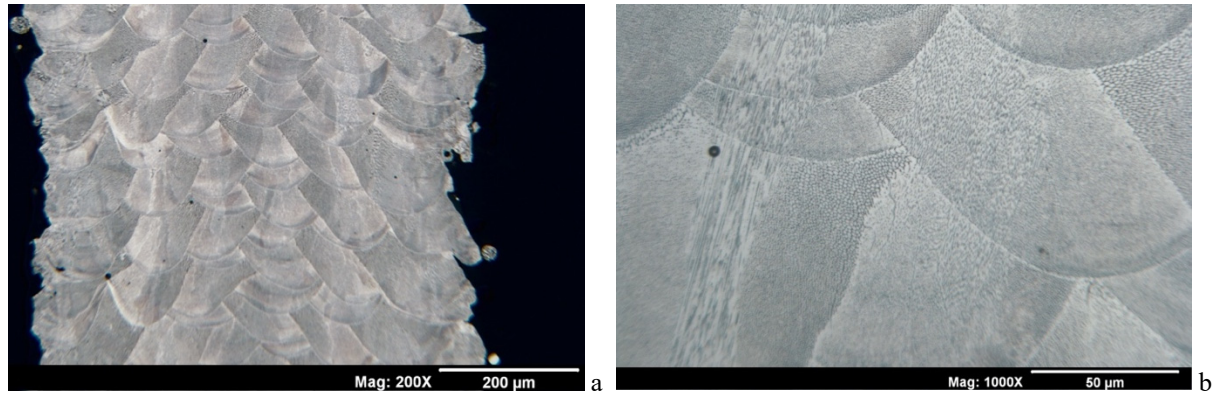


Figure 11. The microstructure of a metallographically prepared section along the build direction (bottom-to-top) reveals the (a) scalloped grain structure and (b) lamellar intragranular features of the 0.026 in-thick AM 316L plate.

The yield strength along the build direction is generally less than that within the build plane, as seen by the data listed in Table 1. Although there is often an ultra-refinement in grain size at the solidification front, it's the larger grain structure along the load direction that yields initially during deformation. The method selected for quantification of grain size in the x-y build-plane versus the z build-direction will show this solidification effect. In accordance with the postulate of eqn. (B.10), a correlation between grain size and the dimensionless c_{bi} coefficients can be forecast as formulated in eqn. (12) where c_{g3} represents the dimensional coefficient that corresponds with the Stage 3 softening coefficient c_{b3} .

$$h_g = c_{gi} \cdot c_{bi} \quad (12)$$

The use of the c_{b3} coefficient provides a measure that's readily tractable from the tensile tests to provide a microstructural scale as plotted in Figure 8. In concept, the strength of a material is known to increase as the size of the grain structure decreases, since grain boundaries are obstacles to plastic deformation from dislocation motion in accordance with the rationale presented in Appendix B. As such the larger the grains, the more readily the material deforms, producing a rapid descent in $\Theta(\sigma)$ as stress σ increases and resulting in a greater c_{b3} value than for smaller grains. This result produces the trends observed in Figure 8 and the formulation of eqn. (12).

4. Discussion

The current modelling approach unifies the attributes common to the work hardening behavior of alloys. The onset of plastic deformation corresponds with the mobilization of dislocations beyond the elastic range of stress-strain $\sigma(\epsilon)$ behavior. The increase in the number of dislocations, as attributable to generation mechanisms such as Frank-Read sources, is associated with the rapid descent in the work hardening $\Theta(\sigma)$ curve and the classic use of the Hollomon $\sigma(\epsilon)$ expression. The saturation of dislocations within the microstructure, i.e. the near balance of dislocation generation with annihilation, as the sample undergoes extended uniform elongation is associated with a classic use of the Voce $\sigma(\epsilon)$ relationship. The onset of additional work hardening mechanisms as twinning induced plasticity, often associated with an intermittent leveling of the $\Theta(\sigma)$ curve during its descent, is detailed in the constitutive formulations of Appendix A. The use of superposition in the negative-exponential formulation for $\Theta(\sigma)$ provides the means to envelope and quantify the beginning and ending stages of work hardening behaviors. Specifically, a significant increase in the magnitude of the (c_{bi}, c_{ij}) coefficients is found for Stage 3 (dislocation onset and increase) versus Stage 4 (near steady-state dislocation behavior) that accounts for the differences in work hardening mechanisms using one base formulation, and a means to quantify differences that distinguish alloy systems. Intrinsic to the work hardening mechanism is the formulation for the softening coefficient c_{b3} that provides an equivalence to grain size in its relationship with strength as detailed by the Appendix B formulations. These unique mechanism contributions to the work hardening behavior are now quantifiable over the specific ranges of stress in which they occur, including intermittent behaviors. The ability to quantify differences between the work hardening mechanisms as attributable to composition within an alloy system should be possible with this unified approach. The ability to distinguish transformation induced phases during

work hardening should be possible as well, including quantification of phase changes that may occur as plastic deformation proceeds to fracture beyond the structural instability.

The wrought 316L material represents an upper bound in the refinement of the softening coefficient c_b and the achievement of greater plasticity ε_p as obtainable in the additively manufactured 316L samples. These attributes are seen in the plots of Figs. 1-2 and the data listed in Table 1. The use of a negative-exponential formulation for the work hardening in eqn. (2) provides a means to encapsulate the observed fluctuations in the $\Theta(\sigma)$ behavior attributable in the onset of deformation and through the progression of dislocation motion behavior. This approach provides a means to model plastic deformation from its onset to the strength instability. These attributes for work hardening as seen in Figs. 3 and 6 are integral to a commensurate formulation in eqn. (4) of the stress-strain model that proves useful to account for the transition from rapid work hardening through the steady state range to the strength instability as seen in Figure 7. Despite the noise observed in experimental data, the relationship between Stages 3 and 4 as formulated from eqn. (3) is verified in the Figure 5 plot of the softening coefficients c_{bi} wherein an exponential decrease in c_{b3} accompanies the increase in the c_{b4} value, as strength increases between samples.

The observation is made that the softening coefficient, which demarks the onset of plasticity, can be used as a surrogate for a microstructural assessment of grain size as formulated in the eqn. (B.10) Hall-Petch formulation of strength. This postulate is validated in the Figure 8 plot of strength data for the complex solidified growth structure of AM 316L as seen in Figure 11. The result is consistent with prior reporting (Jankowski 2024) from a sampling of archival mechanical behavior reported for AM Ti-6Al-4V. Future efforts to determine the c_{gi} coefficient of eqn. (12) for a material system will establish a direct means to directly quantify microstructural scale using stress-strain behavior.

The softening coefficient c_{b3} for the onset of deformation from Stage 3 is related to the activation volume v^* for the onset of dislocation motion as presented in eqns. (9-10). Results for the AM 316L samples of Tables 1 and 2 are plotted in Figure 9 that demonstrate the linear relationship between these variables. Commensurate with the Hall-Petch postulate of eqn. (B.10) and the activation volume v^* formulation as a function of c_{b3} , a parabolic decay in v^* is predicted by eqn. (11) and observed in the Figure 10 plot of experimental data.

The coefficients to the work hardening and stress-strain formulations shown in eqns. (2-5) are determined from a mathematical fit to the data trend that originates at the instability stress in the work hardening plot and traces with decreasing σ -values to the yield strength at the proportional limit. Unlike a linear Kocks-Mecking (K-M) fit for $\Theta(\sigma)$ that corresponds to the Voce stress-strain formulation, the present work hardening model accommodates the actual curvilinear behavior within the steady-state Stage 4 of plastic deformation as well as the rapid work hardening of Stage 3. The consistency between evaluating the c_{bi} coefficients between the linear K-M approximation and the curvilinear $\Theta(\sigma)$ formulation of eqn. (2) is seen in Figure 4 as evaluated at the proportional limit and at the strength instability. The c_{1j} and c_{2j} coefficients are uniquely determined in this method to the negative exponential formulation of eqn. (2) for each work hardening stage. These c_{ij} coefficients are used to compute the c_{oj} coefficient value of eqn. (5) as, e.g., at the proportional limit and instability for the Stages 3 and 4 formulations, respectively. Using these coefficients, the work hardening and stress-strain curves can be simulated using the model formulation of eqns. (7) and (8), respectively. Since the $\Theta(\sigma)$ curves are often statistically noisy, i.e. from oscillations in loading that typically accompany strain-rate controlled testing, the c_{ij} coefficients can be refined through iteration with the experimental stress-strain behavior. The effect of increasing c_{2j} is to reduce or flatten the slope of the $\sigma(\varepsilon)$ curve. The effect of decreasing c_{1j} is to reduce or lower the $\sigma(\varepsilon)$ values. The c_{oj} value will commensurately change with c_{1j} and c_{2j} values, in accordance with eqn. (5), and effectively translates the $\sigma(\varepsilon)$ curve to higher or lower values while preserving curve shape.

Further development of the current approach, that envelopes the work hardening behavior from Stage 3 and 4 with an integral unifying model of stress-strain behavior, to include post yield work hardening behaviors is demonstrated in Appendix A. Herein, an additional Gaussian component of work hardening is introduced in eqn. (A.1) that completes a full modeling of the nuanced $\Theta(\sigma)$ behavior (as shown in Figure A.1) which leads to the eqn. (A.9) series solution in a $\varepsilon(\sigma)$ formulation enabling a full duplication of the entire true stress-strain behavior (as shown in Figure A.2) from the proportional limit to the instability.

5. Summary

A new approach to assess the work hardening behavior $\Theta(\sigma)$ is presented using a series solution based on a negative-exponential formulation of stress. This approach can be used to model plasticity from the onset of deformation to the strength instability. In this case study, application is demonstrated from the proportional limit to localized necking for wrought and AM 316L tensile samples. The assessment of the softening coefficients c_{bi} , often associated with a Voce-type assessment of work hardening in the steady state range of plastic deformation,

proves enabling for evaluating strengthening over the entire range of stress-strain behavior. As proposed to be representative of the refinement in microstructural scale for strengthening steels to the nanoscale, as first proposed by J.W. Morris, Jr. (2007), the c_{bi} parameters have been analytically related (Jankowski 2023) to dislocation activation volume v^* , strain rate sensitivity $\dot{\epsilon}$, and to a Hall-Petch type-formulation (Jankowski 2024) of strength σ . This method provides a means to quantify the qualification process that accommodates the complex solidified microstructure of additively manufactured materials as reported (Jankowski, et al. 2020) for 316L AM material.

Acknowledgments

This work was inspired by the objective to enhance the engineering application of structural AM materials. Prior collaborative and joint work with colleagues N. Yang, W-Y. Lu, and A. Gardea at Sandia Livermore was integral for inspiring the modeling and data analysis pursued in this presentation. Any subjective views or opinions that might be expressed in the paper do not necessarily represent the views of the US Department of Energy or the United States Government. Sandia National Laboratories is a multi-mission laboratory managed and operated by National Technology & Engineering Solutions of Sandia, LLC, a wholly owned subsidiary of Honeywell International Inc, for the US Department of Energy's National Nuclear Security Administration under contract DE-NA0003525. Data from which the modeling and simulations in this paper are made is available in the literature referenced and upon request.

Key Terms and Acronyms

additively manufactured (AM)
 electron beam melting (EBM)
 selective laser melting (SLM)
 direct metal laser sintering (DMLS)
 face center cubic (fcc)
 hexagonal close packed (hcp)
 Boltzmann's constant (k_B)
 temperature absolute (T)
 elastic Young's modulus (E)
 true strength (σ_i)
 true strain (ϵ_i)
 plastic strain (ϵ_p)
 yield strength at proportional limit (σ_y)
 ultimate strength at plastic instability (σ_u)
 yield-to-ultimate strength ratio (σ_y^*)
 stress at transition between stages 3 and 4 of work hardening (σ_d)
 softening coefficient (c_b)
 softening coefficient in stage "i" of work hardening (c_{bi})
 plastic strain in stage "i" of work hardening (ϵ_{pi})
 work hardening in stage "i" of work hardening (θ_i)
 intercept of work hardening at zero stress in stage "i" of work hardening (θ_{oi})
 strain rate ($\dot{\epsilon}$)
 strain-rate sensitivity-of-strength exponent (m)
 activation volume (v^*) and activation volume coefficient (c_{v^*})
 standard deviation (δ) and mean value (μ) of the work hardening Gaussian (θ) function

References

- Cahn, J. W., & Nabarro, F. R. N. (2001). Thermal activation under shear. *Philosophical Magazine A*, 81(5), 1409-1426. <https://doi.org/10.1080/01418610108214448>
- Chen, J., Lu, L., & Lu, K. J. S. M. (2006). Hardness and strain rate sensitivity of nanocrystalline Cu. *Scripta Materialia*, 54(11), 1913-1918. <https://doi.org/10.1016/j.scriptamat.2006.02.022>
- Gibbs, G. B. (1969). Thermodynamic Analysis of Dislocation Glide Controlled by Dispersed Local Obstacles. *Mater Sci Eng.*, 4, 313-328. [https://doi.org/10.1016/0025-5416\(69\)90026-3](https://doi.org/10.1016/0025-5416(69)90026-3)
- Hilliard, J. E. (1964). Estimating Grain Size by the Intercept Method. *Metal Progress*, 85(5), 99-102.
- Hollomon, J. H. (1945). Tensile Deformation. *Trans AIME*, 162, 268-290.
- Jankowski, A. F., & Wilford, T. O. (1987). Grain Size Variation in Coatings. *J. Metals*, 39(6), 28-30. <https://doi.org/10.1007/BF03258058>

- Jankowski, A. F., Ferreira, J. L., & Hayes, J. P. (2005). Activation Energy for Grain Growth in Aluminum Coatings. *Thin Solid Films*, 491, 61-65. <https://doi.org/10.1016/j.tsf.2005.05.027>
- Jankowski, A. F., Chames, J. M., Gardea, A., Nishimoto, R., & Brannigan, E. M. (2019). The softening factor c_b of commercial titanium alloy wires. (Zeitschrift fuer Metallkunde). *International Journal of Materials Research*, 110, 990-999. <https://doi.org/10.3139/146.111834>
- Jankowski, A. F., Yang, N., & Lu, W-Y. (2020). Constitutive structural parameter c_b for the work hardening behavior of laser powder-bed fusion, additively manufactured 316L stainless steel. *Material Design and Processing Communication*, 2020, e96-1-9. <https://doi.org/10.1002/mdp2.135>
- Jankowski, A. F. (2021). A constitutive structural parameter c_b for the work hardening behavior of additively manufactured Ti-6Al-4V. *Material Design and Processing Communication*, 2021, e262-1-9. <https://doi.org/10.1002/mdp2.262>
- Jankowski, A. F. (2023). On the origin of stress-strain relationships, the evaluation if softening coefficients and mechanistic models for work hardening. *Materials Science and Engineering A*, 882, 145472-1-14. <https://doi.org/10.1016/j.msea.2023.145472>
- Jankowski, A. F., & Yee, J. K. (2023). Stress-strain and work hardening relationships of 304L AM alloy. *Sandia National Laboratory SAND2023-11259*, 33 pages. <https://doi.org/10.2172/2430159>
- Jankowski, A. F. (2024). On the onset of plasticity: determination of strength and ductility. *Journal of Materials Science Research*, 13(1), 16-27. <https://doi.org/10.5539/jmsr.v13n1p16>
- Kocks, U. F., & Mecking, H. (2003). Physics and phenomenology of strain hardening: the FCC case. *Progress in Materials Science*, 48, 171-273. [https://doi.org/10.1016/S0079-6425\(02\)00003-8](https://doi.org/10.1016/S0079-6425(02)00003-8)
- Li, J. C. M., & Chou, Y. T. (1970). The role of dislocation in flow stress grain size relationships. *Met. Trans., 1*, 1145-1159. <https://doi.org/10.1007/BF02900225>
- Morris, Jr., J. W. (2007). Is there a future for nanostructured steel? in 16th International Society for Offshore and Polar Engineering Conf. Proc. *ISOPE*, 2007, 2814-2818.
- Voce, E. (1948). The Relationship Between Stress and Strain for Homogeneous Deformation. *J. of the Institute Metals*, 74, 537-562.
- Wang, S., Li, J., Cao, Y., Gao, B., Mao, Q., & Li, Y. (2018). Thermal stability and tensile property of 316L stainless steel with heterogeneous lamella structure. *Vacuum*, 152, 261-4. <https://doi.org/10.1016/j.vacuum.2018.03.040>
- Zhu, Q., Zhao, Q., Huang, Q., Chen, Y., Suresh, S., Yang, W., ... & Wang, J. (2024). Grain boundary plasticity initiated by excess volume. *Proc. Nat. Acad. Sci.*, 121(12), e2400161121. <https://doi.org/10.1073/pnas.2400161121>

Appendices

Appendix A

A Gaussian expression can be used for the work hardening stage $\theta(\sigma)$ of plasticity that corresponds to, e.g., partial dislocation motion, dislocation glide, or twinning. In the eqn. (A.1) formulation, δ is the standard deviation, μ is the mean value, and θ_o is the amplitude of the Gaussian work hardening stage.

$$\theta(\sigma) = \left(\frac{\partial \sigma}{\partial \varepsilon} \right) = \frac{\theta_o}{\delta \sqrt{2\pi}} e^{-\frac{1}{2}[(\sigma-\mu)/\delta]^2} \quad (\text{A.1})$$

This portion of work hardening is superimposed upon the use of eqn. (7) for establishing the baseline envelope for $\theta(\sigma)$ from Stage 3 and 4 contributions. An integral form of eqn. (A.1) for the discrete stage of plasticity can be used to arrive at an expression for the corresponding strain-stress equation, by solving eqn. (A.1) for the true strain as a function of true stress $\varepsilon(\sigma)$.

$$\int \partial \varepsilon = \int \frac{\delta \sqrt{2\pi}}{\theta_o} e^{\frac{1}{2}[(\sigma-\mu)/\delta]^2} \partial \sigma \quad (\text{A.2})$$

Equation (A.2) can be simplified using the following variable substitutions.

$$C_1 = \left(\frac{1}{2\delta^2} \right) \quad (\text{A.2a})$$

$$C_2 = \left(\frac{\delta \sqrt{2\pi}}{\theta_o} \right) \quad (\text{A.2b})$$

$$x = (\sigma - \mu) \quad (\text{A.2c})$$

$$\partial x = \partial \sigma \quad (\text{A.2d})$$

Equations (A.2a-d) are substituted in eqn. (A.2) to arrive at the following integral for strain ε .

$$\varepsilon = C_2 \int e^{C_1 x^2} \partial x \quad (\text{A.3})$$

The exponent of eqn. (A.3) can be simplified by the following substitution.

$$y = x^2 = (\sigma - \mu)^2 \quad (\text{A.3a})$$

$$\partial y = 2x \partial x \quad (\text{A.3b})$$

$$\partial x = \left(\frac{\partial y}{2x} \right) = \left(\frac{\partial y}{2\sqrt{y}} \right) \quad (\text{A.3c})$$

Equation (A.3) can be rewritten through substitution of eqns. (A.3a-c).

$$\varepsilon = C_2 \int \frac{1}{2\sqrt{y}} e^{C_1 y} \partial y \quad (\text{A.4})$$

Equation (A.4) can be solved by using the method of integration by parts (u, v). That is, eqn. (A.4) can be rewritten according to the formulation where $\int u \partial v$ equals $uv - \int v \partial u$, wherein the variables u and v are defined in eqns. (A.4a-d).

$$u = e^{C_1 y} \quad (\text{A.4a})$$

$$\partial u = C_1 e^{C_1 y} \quad (\text{A.4b})$$

$$\partial v = \left(\frac{\partial y}{2\sqrt{y}} \right) \quad (\text{A.4c})$$

$$v = \sqrt{y} \quad (\text{A.4d})$$

The variables (u, v) of eqns. (A.4a-d) are next substituted into equation (A.4).

$$\varepsilon = C_2 \left[\sqrt{y} e^{C_1 y} - \int \sqrt{y} C_1 e^{C_1 y} \partial y \right] \quad (\text{A.5})$$

The integral in eqn. (A.5) can be solved by once again using the method of integration by parts, where the (u, v)

variables are now defined in eqns. (A.5a-d).

$$u = e^{C_1 y} \quad (\text{A.5a})$$

$$\partial u = C_1 e^{C_1 y} \partial y \quad (\text{A.5b})$$

$$\partial v = C_1 \sqrt{y} \partial y \quad (\text{A.5c})$$

$$v = \frac{2}{3} C_1 y^{\frac{3}{2}} \quad (\text{A.5d})$$

The variables (u, v) of eqns. (A.5a-d) are now substituted into equation (A.5).

$$\begin{aligned} \varepsilon &= C_2 \left[\sqrt{y} e^{C_1 y} - \left(e^{C_1 y} \frac{2}{3} C_1 y^{\frac{3}{2}} - \int \frac{2}{3} C_1 y^{\frac{3}{2}} C_1 e^{C_1 y} \partial y \right) \right] \\ &= C_2 \left[e^{C_1 y} \left(\sqrt{y} - \frac{2}{3} C_1 y^{\frac{3}{2}} \right) + \int \frac{2}{3} C_1^2 y^{\frac{3}{2}} e^{C_1 y} \partial y \right] \end{aligned} \quad (\text{A.6})$$

The integral of eqn. (A.6) can be solved by another iteration using the method of integration by parts, where the (u, v) variables are now defined in eqns. (A.6a-d).

$$u = e^{C_1 y} \quad (\text{A.6a})$$

$$\partial u = C_1 e^{C_1 y} \partial y \quad (\text{A.6b})$$

$$\partial v = \frac{2}{3} C_1^2 y^{\frac{3}{2}} \partial y \quad (\text{A.6c})$$

$$v = \frac{4}{15} C_1^2 y^{\frac{5}{2}} \quad (\text{A.6d})$$

The variables (u, v) of eqns. (A.6a-d) are then substituted into equation (A.6).

$$\begin{aligned} \varepsilon &= C_2 \left[e^{C_1 y} \left(\sqrt{y} - \frac{2}{3} C_1 y^{\frac{3}{2}} \right) + \left(e^{C_1 y} \frac{4}{15} C_1^2 y^{\frac{5}{2}} - \int \frac{4}{15} C_1^2 y^{\frac{5}{2}} C_1 e^{C_1 y} \partial y \right) \right] \\ &= C_2 \left[e^{C_1 y} \left(\sqrt{y} - \frac{2}{3} C_1 y^{\frac{3}{2}} + \frac{4}{15} C_1^2 y^{\frac{5}{2}} \right) - \int \frac{4}{15} C_1^2 y^{\frac{5}{2}} C_1 e^{C_1 y} \partial y \right] \end{aligned} \quad (\text{A.7})$$

It's clear that a series expansion is developing in eqn. (A.7). Another iteration of the method of integration by parts using the variables (u, v) of eqns. (A.7a-d) as substituted into equation (A.7) will reveal the general solution to eqn. (A.4) in the form of a series expansion.

$$u = e^{C_1 y} \quad (\text{A.7a})$$

$$\partial u = C_1 e^{C_1 y} \partial y \quad (\text{A.7b})$$

$$\partial v = \frac{4}{15} C_1^3 y^{\frac{5}{2}} \partial y \quad (\text{A.7c})$$

$$v = \frac{8}{105} C_1^3 y^{\frac{7}{2}} \quad (\text{A.7d})$$

The variables (u, v) of eqns. (A.7a-d) are substituted into equation (A.7).

$$\begin{aligned} \varepsilon &= C_2 \left[e^{C_1 y} \left(\sqrt{y} - \frac{2}{3} C_1 y^{\frac{3}{2}} + \frac{2}{5} \cdot \frac{2}{3} C_1^2 y^{\frac{5}{2}} - \frac{2}{7} \cdot \frac{2}{5} \cdot \frac{2}{3} C_1^3 y^{\frac{7}{2}} \right) + \int \frac{2}{7} \cdot \frac{2}{5} \cdot \frac{2}{3} C_1^3 y^{\frac{7}{2}} C_1 e^{C_1 y} \partial y \right] \\ &= C_2 e^{C_1 y} \left[\sqrt{y} - \frac{2}{3} C_1 y^{\frac{3}{2}} + \frac{4}{15} C_1^2 y^{\frac{5}{2}} - \frac{8}{105} C_1^3 y^{\frac{7}{2}} + \frac{16}{945} C_1^4 y^{\frac{9}{2}} - \dots \right] \\ &= \sum_0^n (-1)^n \frac{2^n}{(2n+1)!} C_1^n y^{\frac{2n+1}{2}} C_2 e^{C_1 y} \end{aligned} \quad (\text{A.8})$$

The substitution of terms for C_1 , C_2 , and y from eqns. (A.2a-b, A.3a) into eqn. (A.8) arrives at the final solution

for $\varepsilon(\sigma)$ as seen in eqn. (A.9).

$$\varepsilon = \sum_0^n \left[(-1)^n \frac{1}{(2n+1)!} \left(\frac{1}{\delta^2} \right)^n (\sigma - \mu)^{2n+1} \left(\frac{\delta\sqrt{2\pi}}{\theta_0} \right) e^{\frac{1}{2}[(\sigma-\mu)/\delta]^2} \right] \quad (\text{A.9})$$

An application of eqn. (A.9) is applied to the case for the work hardening of sample no. 2 P.066-X2 as shown in Fig. 3. The rapid descent of $\theta(\sigma)$ for Stage 3 as modeled using eqn. (2) is shown in Fig. A.1a and the shallow curvilinear behavior of Stage 4 as modeled using eqn. (2) is shown in Fig. A.1b.

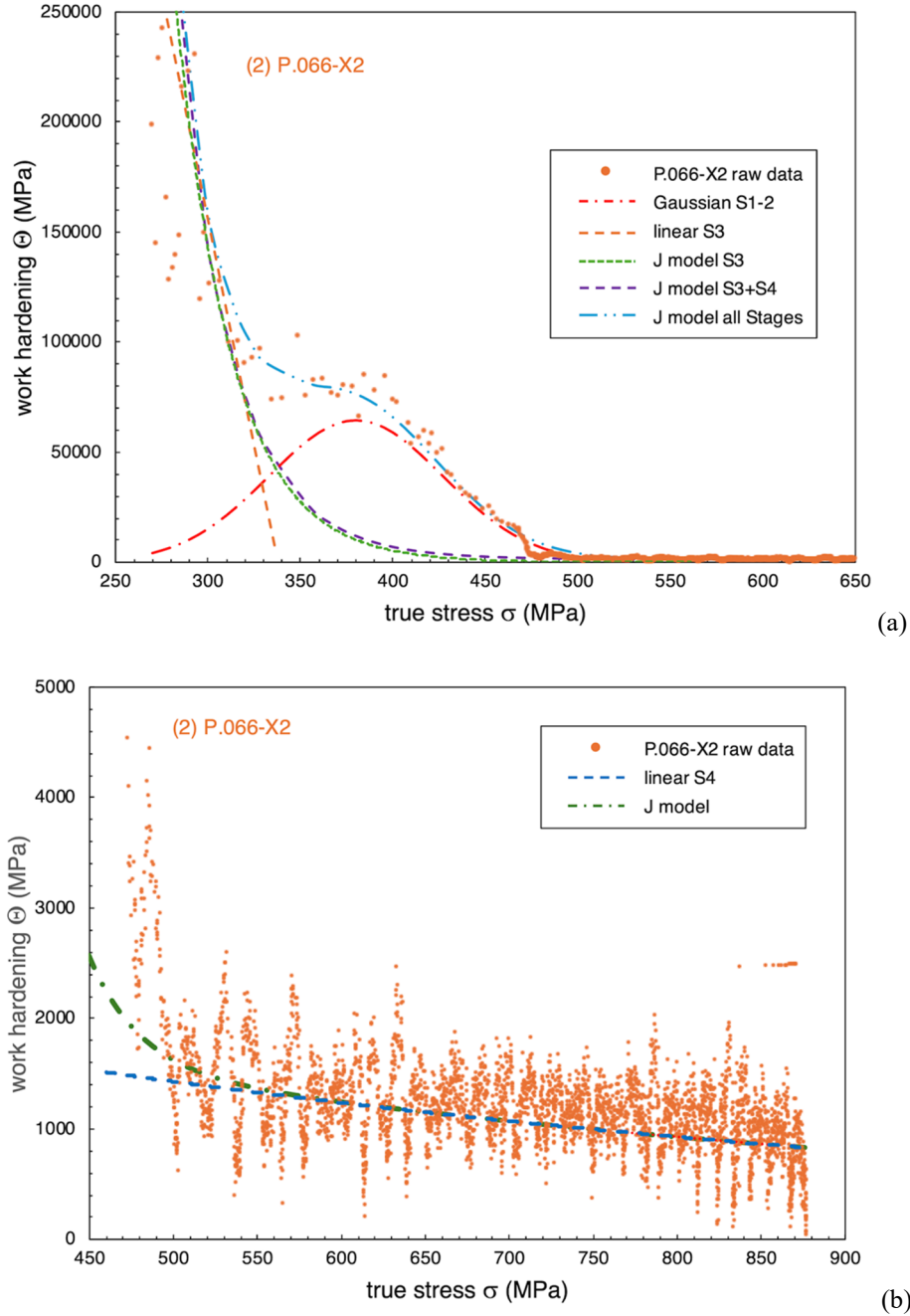


Figure A.1. The work hardening of sample no. 2 P.066-X2 is shown in (a) for all stages including the additional post Stage 3 Gaussian component and (b) the Stage 4 component.

The c_{ij} coefficients computed for each stage are listed in Table 1, accordingly. The $\theta(\sigma)$ components for Stages

3 and 4 are shown individually and as summed using eqn. (7). The Gaussian portion for the additional work hardening component is shown separately (for the stress σ input range of 270 to 530 MPa) where the eqn. (A.1) values for the standard deviation δ , mean value μ , and amplitude θ_o equals 47, 380, and 7600 MPa, respectively. This portion of work hardening has been referred (Kocks and Mecking 2003) to as Stage 1-2 behavior and is here summed with the Stage 3 and 4 components as shown in Fig. A.1a for the $\theta(\sigma)$ curve fit of all stages. The input of all the work hardening parameters into eqn. (8) produces the true stress-strain $\sigma(\varepsilon)$ curves show in Fig. A.2. In this $\sigma(\varepsilon)$ plot, the contribution from each plasticity stage is shown, including that of the Gaussian portion shown in Fig. A.1a. The inclusion of the $\sigma(\varepsilon)$ contribution from Stage 1-2 is seen to close the gap to the actual experimental $\sigma(\varepsilon)$ data from the fit estimated using the Stage 3+4 input. To note, the $\theta(\sigma)$ and $\sigma(\varepsilon)$ curve fits for this sample have not been optimized for full convergence onto the experimental results but do illustrate the process and application of the formulations introduced in this Appendix.

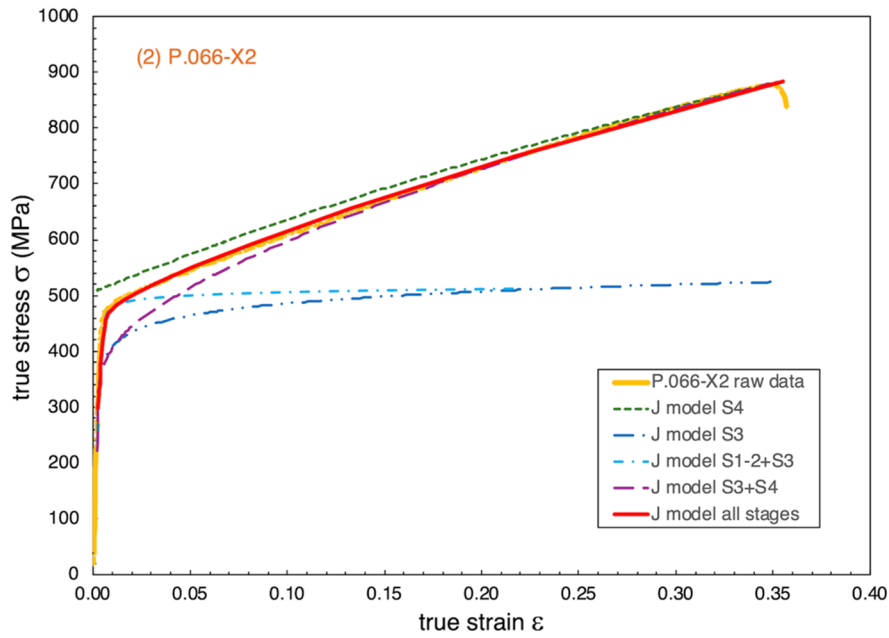


Figure A.2. The simulation of true stress-strain behaviors for individual and collective work hardening stages of sample no. 2 P.066-X2.

Appendix B

The analytic derivation of the Hall-Petch relationship is shown, as shared by J. W. Morris, Jr., and now developed under the assumption that the softening coefficient c_{b3} represents a measure of the microstructural scale at the yield point. As c_{b3} and c_{b4} are shown to be related through the work hardening expression through eqn. (3), a formalism for the Hall-Petch construct can then be derived that utilizes the c_{b4} coefficient, noting that this coefficient can often be more readily measured from $\theta(\sigma)$ behavior.

Grain boundaries are barriers to dislocation motion (Chen, et al. 2006, Zhu, et al. 2024) wherein dislocations that are gliding on the same slip plane will pile-up at the edge of a grain which magnifies the applied shear stress τ at the boundary. An equivalence can be expressed for the effective shear stress τ_e under an applied tensile stress σ for n dislocations in the pile-up.

$$\tau_e = n \cdot \tau_i \quad (\text{B.1})$$

Here, τ_i is the resolved shear stress [2], and the number n can be equated as follows where G is the shear modulus, b is the magnitude of the Burgers vector, h is the grain size and κ equals 1 for a screw dislocation or $(1 - n)$ for an edge dislocation (Li and Chou, 1970).

$$n = (\kappa \cdot \pi \cdot \tau_i \cdot h) / (4G \cdot b) \quad (\text{B.2})$$

When the stress in the tip of the pile-up reaches/exceeds a critical stress τ_c , then dislocations are generated in the neighboring grain, slip will continue, and plastic deformation results. The macroscopic plastic deformation is then

the spreading of dislocation activity throughout the specimen, and the critical stress at which this occurs is equated as follows.

$$\tau_c = \tau_e = n \cdot \tau_i \quad (\text{B.3})$$

By substituting eqn. (B.2) into (B.3), the critical stress is related to grain size.

$$\tau_c = (\kappa \cdot \pi \cdot \tau_i^2 \cdot h) / (4G \cdot b) \quad (\text{B.4})$$

The resolved shear stress τ_i required to overcome the influence of the grain boundary is the applied stress τ less the friction stress to overcome intrinsic resistance τ_o .

$$\tau_i = \tau - \tau_o \quad (\text{B.5})$$

Upon substituting eqn. (B.5) into (B.4), the critical shear stress is computed.

$$\tau_c = n \cdot \tau_i = [\kappa \cdot \pi \cdot (\tau - \tau_o)^2 \cdot h] / (4G \cdot b) \quad (\text{B.6})$$

Equation (B.6) can then be solved for determining stress τ as a function of grain size h by: multiplying eqn. (B.6) by $4G \cdot b$ in eqn. (B.7a); dividing by $\kappa \cdot \pi \cdot h$ in eqn. (B.7b); taking a square-root in eqn. (B.7c); and solving for real solutions of stress τ in eqn. (B.7d).

$$(4G \cdot b) \cdot \tau_c = n \cdot \tau_i = [\kappa \cdot \pi \cdot (\tau - \tau_o)^2 \cdot h] \quad (\text{B.7a})$$

$$(4G \cdot b) \cdot \tau_c / (\kappa \cdot \pi \cdot h) = (\tau - \tau_o)^2 \quad (\text{B.7b})$$

$$(\tau - \tau_o) = \pm [(4G \cdot b) \cdot \tau_c / (\kappa \cdot \pi \cdot h)]^{\frac{1}{2}} \quad (\text{B.7c})$$

$$\tau = \tau_o + [(4G \cdot b) \cdot \tau_c / (\kappa \cdot \pi)]^{\frac{1}{2}} \cdot h^{-\frac{1}{2}} \quad (\text{B.7d})$$

The familiar form of the Hall-Petch expression is then shown in eqn. (B.8) where the critical-resolved stress coefficient k_τ equals $\sqrt{(4G \cdot b) \cdot \tau_c / (\kappa \cdot \pi)}$, or by using the tensile stress σ equivalent in equation (B.9).

$$\tau = \tau_o + k_\tau \cdot h^{-\frac{1}{2}} \quad (\text{B.8})$$

$$\sigma = \sigma_o + k_\sigma \cdot h^{-\frac{1}{2}} \quad (\text{B.9})$$

It's postulated that the c_{bi} coefficient can be substituted as a measure for microstructural size in the Hall-Petch relationship of eqn. (B.9) at the proportional limit σ_p .

$$\sigma_p = k_\sigma \cdot \left(\frac{1}{\sqrt{c_{b3}}} \right) + \sigma_{op} \quad (\text{B.10})$$

The c_{bi} coefficients for Stages 3 and 4 can be related (Jankowski 2024) according to the following expression assuming a negative exponential relationship between these variables.

$$c_{b4} = c_{3j} \cdot e^{-c_{4j} \cdot c_{b3}} \quad (\text{B.11})$$

The above eqn. (B.11) can be solved for c_{b3} , accordingly.

$$\ln c_{b4} = \ln(c_{3j} \cdot e^{-c_{4j} \cdot c_{b3}}) \quad (\text{B.12a})$$

$$\ln c_{b4} = \ln c_{3j} + \ln(e^{-c_{4j} \cdot c_{b3}}) \quad (\text{B.12b})$$

$$\ln c_{b4} = \ln c_{3j} - c_{4j} \cdot c_{b3} \quad (\text{B.12c})$$

$$c_{4j} \cdot c_{b3} = \ln c_{3j} - \ln c_{b4} \quad (\text{B.12d})$$

$$c_{b3} = \left(\frac{1}{c_{4j}} \right) \cdot \ln \left(\frac{c_{3j}}{c_{b4}} \right) \quad (\text{B.12e})$$

Eqn. (B.12e) can now be substituted into eqn. (B.10).

$$\sigma_p = k_\sigma \cdot \left[\left(\frac{1}{c_{4j}} \right) \cdot \ln \left(\frac{c_{3j}}{c_{b4}} \right) \right]^{-\frac{1}{2}} + \sigma_{op} \quad (\text{B.13})$$

From a plot of c_{b4} as a function of c_{b3} , the coefficients c_{3j} and c_{4j} can be determined to then establish a linear plot of $(1/c_{4j}) \cdot \ln(c_{3j}/c_{b4})^{-1/2}$ versus σ_p , provided the Hall-Petch relationship is a valid function of c_{bi} .

Copyrights

Copyright for this article is retained by the author(s), with first publication rights granted to the journal.

This is an open-access article distributed under the terms and conditions of the Creative Commons Attribution license (<http://creativecommons.org/licenses/by/4.0/>).